Evaluation of hepatotoxic effects of acetaminophen on HepG2 cells by parallel real-time monitoring in a multi-sensor analysis platform for automated cell-based assays

[ORCID] Christina Heichler[1], [ORCID] Márton Nagy[1], Peter Wolf[1*]

1 INCYTON GmbH, Am Klopferspitz 19A, 82152 Planegg/Martinsried, Germany
* Corresponding authors: peter.wolf@incyton.com

Abstract

The CYRIS® analysis platform is a multi-sensory approach to extract a large amount of information from a single cell-based assay automatically and in real-time. To demonstrate its capabilities, we performed an in-vitro hepatotoxicity assay with Acetaminophen and HepG2, with simultaneous monitoring of the key parameters oxygen consumption rate (OCR), extracellular acidification rate (ECAR), impedance and microscopic imaging. After 12 hours prior treatment measurement, different concentrations of Acetaminophen were tested over 24 hours, followed by 12 hours washout. The metabolic results showed a strong time- and dose-dependent change of OCR and ECAR through Acetaminophen. Morphologic changes monitored by impedance and microscopic imaging underpin these metabolic effects. The washout of Acetaminophen results in cellular regeneration in all parameters up to a concentration of 10 mM. The continuous measurement of OCR, ECAR, impedance and microscopic imaging enables multiparametric monitoring of cellular metabolic responses due to Acetaminophen in a single assay and provides an overall picture of its hepatotoxic effects.

1. Introduction

Cell-based assays, as performed here, are an in-vitro method used to analyze the reactions of living cell cultures under specific treatment. The aim is to identify the effects of a drug that originate from specific combinations of drug concentrations and treatment times. In addition, conclusions can be drawn about the mechanism of action underlying the drug effects and the modulation of these effects by repeated treatment and washout sequences. Knowledge of adverse effects of a drug, especially at higher doses, is the basis for drug safety assessment in pre-clinical testing to reduce the risk of adverse effects in the clinic. In this context, the issue of drug-induced liver injury (DILI) has become particularly important in recent years. Therefore, cell-based assays can reduce the costs of failure in drug development by detecting negative effects early, long before a patient comes into contact with a drug. In addition, cell-based assays with a well-chosen cell model are fundamentally suited to replace or minimize animal testing, which is often required by law. Last but not least, ethical reasons also speak in favor of conducting basic research on cell models as far as possible. Given these basic assumptions and a strong trend towards automation, a project was driven to develop an automated platform for cell-based assays that uses a multi-sensory approach (dissolved oxygen, pH, impedance, microscopic imaging) to extract a large amount of information from a single experiment while controlling all environmental parameters (temperature, humidity, gas atmosphere, treatment regimen). There are various systems on the market that capture different combinations of dissolved oxygen, pH and impedance parameters in immediate environment of live cells in a single chip or multi-well approach and with different drug delivery options (Ferrick et al 2008; Thedinga et al 2007; Wiest et al 2006). However, none of them integrate automated imaging and full atmospheric environmental control in a single instrument. Here we use our latest development, the CYRIS® FLOX analysis platform, to demonstrate its strengths in (hepato-)toxic assays.

Therefore, we investigate the hepatotoxic effects of Acetaminophen (APAP) on a common human hepatocarcinoma-derived cell line (HepG2) that is well suited for basic hepatotoxic studies. APAP is also known as Paracetamol and is one of the most commonly used drugs for pain and fever. However, the DILI risk of APAP is well recognized (Albrecht et al 2019; Chen et al 2016) and APAP-induced liver damage (Lee 2003) is one of the most prevalent causes of acute liver failure (Lee 2013). To demonstrate the dose- and time-dependent effects, this assay tests high potency (50 mM), medium potency (10 mM) and low potency (5 mM and 1 mM) concentrations against a control group (0 mM) over a 24 hour treatment period. The completely automated experiment procedure, in which the calculated oxygen consumption rate (OCR) and extracellular acidification rate (ECAR), as well as periodic microscopic imaging and cell-related impedance of 24 independent cell samples are examined in parallel, also includes a 12-hour prior treatment measurement and a 12-hour washout period.

2. Material and Methods

2.1. Cell analysis platform CYRIS® FLOX

The automated cell analysis platform CYRIS® FLOX (Figure 1) enables the real-time monitoring of living cells and is the further developed and market-ready version of a previous platform prototype (Wolf et al 2013; Lob et al 2007; Wolf et al 1998). The

underlying technologies and evaluation of metabolic rates from raw data have been previously described in detail (Wolf et al 2013). Using CYRIS® FLOX, complex cellular relationships can be understood by simultaneously observing and calculating several key metabolic parameters, such as dissolved oxygen, oxygen consumption rate, pH, and extracellular acidification rate. In parallel with these metabolic parameters, the analysis platform continuously monitors cellular impedance, which provides quantitative information on cell density and adhesion, and microscopic images of all cultures through a fully automated digital microscope on a high-precision XY stage. These morphological sensors enable the observation of changes in cell density, shape, size and structure, which are further determinants of cell viability.

2.2. Cell culture and hepatotoxicity assay preparation

HepG2 cells (human hepatocarcinoma cell line) are maintained in culture medium (DMEM High Glucose w/ L-Glutamine w/o Sodium Pyruvate, Biowest) which is supplemented with 10 % fetal bovine serum (FBS, Biowest). In preparation for the assay, cells are detached with Accutase (PAN-Biotech), counted, and seeded at a density of 5×10^4 cells per well (47 mm culture area) into 20 culture wells of a sterile sensor plate. 4 wells are filled with pure culture medium to serve as media control and impedance blank correction. The sensor plate is then incubated for 5 hours under standard conditions in a cell culture incubator to allow the cells to adhere.

Meanwhile, the CYRIS® FLOX analysis platform is set up for the assay. For this purpose, deep well plates (DWPs) with (for treatment) or without (for prior treatment measurement and washout) acetaminophen (APAP, Sigma-Aldrich) at the appropriate concentrations (0 mM, 1 mM, 5 mM, 10 mM, and 50 mM) in standard measurement medium (DMEM High Glucose w/ L-Glutamine w/o Sodium Pyruvate w/o NaHCO3 w/o Phenol Red) supplemented with 10 % FBS were prepared and then acclimatized in the CYRIS® FLOX climate chamber (37 °C, 90 % relative humidity, 21 % O_2). The pipetting robot is equipped with sterile p200 pipet tips.

After sufficient adhesion of the cells, the culture medium is replaced by fresh measurement medium, the special fluidic lid is closed, and the sensor plate is inserted into the platform. The assay setting includes a prior treatment measurement period of HepG2 cells without drug for 12 hours, treatment of the cells with different concentrations of APAP (0 mM, 1 mM, 5 mM, 10 mM, and 50 mM) for the next 24 hours, and a post-treatment washout for 12 hours. By starting the corresponding sequence program, the hepatotoxicity assay is performed automatically, and the acquired data is displayed in real-time. Throughout the assay, OCR and ECAR are recorded, as well as the electrical impedance and morphology based on regular microscope images. This data display is suitable for an initial qualitative assessment of the effect of APAP on the metabolic rates of HepG2 cells. However, further analysis of the data is required for a quantitative analysis.
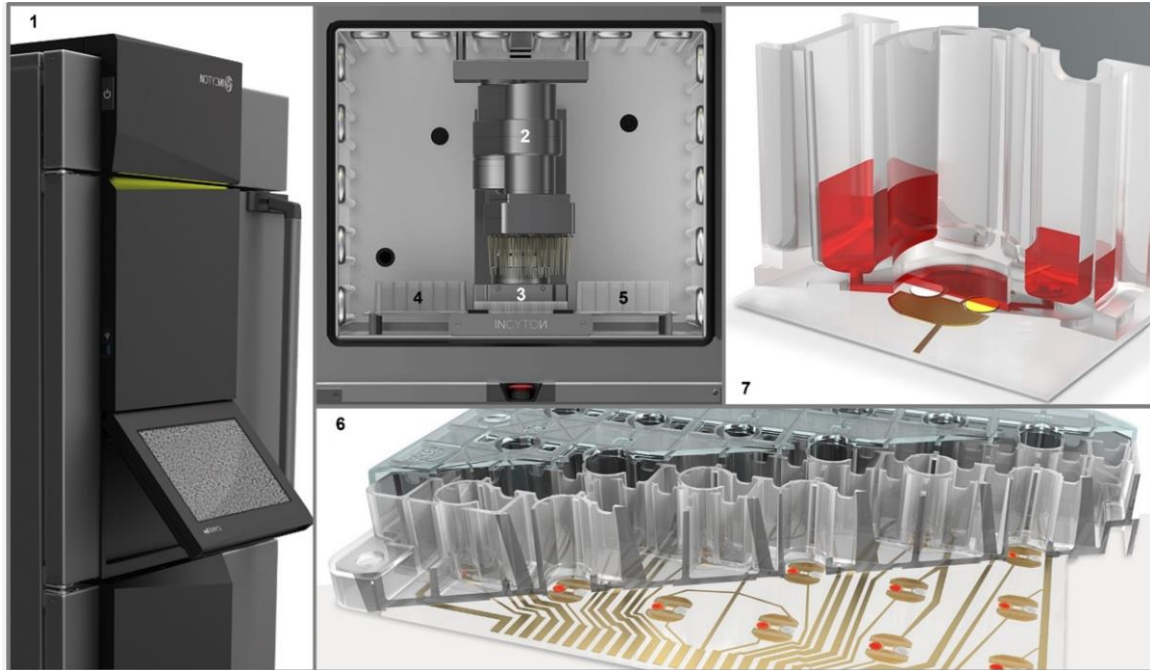
Figure 1. CYRIS® FLOX automated multi-sensor cell analysis platform (1). The platform is equipped with a 24-channel pipetting robot (2), that changes the medium at regular intervals, alternating between the sensor plate (3, 6) and seven flexible positions for deep well plates for storage (4) or waste (5). An automated inverted microscope is positioned below the sensor plate on an XY stage, which is used for optical imaging and relaying the fluorescence readout signal to and from the optical sensors (optrodes) for pH and dissolved oxygen. The sensor plate (6) consists of 24 wells, each constructed as a 3-chamber fluidic system (7) with a central culture chamber equipped with the optrodes and impedance electrodes. The two side chambers are connected to the central culture chamber via microchannels and allow the exchange of media by the robot. By means of a special lid, the volume inside the culture chamber is greatly reduced and sealed from the atmosphere, allowing direct and rapid monitoring of changes in cellular metabolic parameters.

2.3. Data analysis

In principle, metabolic rates were first normalized, i.e., each rate value was divided by the value of the selected normalization time point, usually the time of drug application (t = 12 h). Then, for each individual group (untreated control or treatment with different APAP concentrations), the mean values of the metabolic rates for ECAR and OCR and the standard deviations were calculated. For the quantitative analysis of the impedance data, the same evaluation strategy was used, with an additional normalization step. For this purpose, each individual measured value of cellular impedance was divided by the temporally corresponding mean value of the four media controls without cells (blank correction). EC_{50} values were calculated using the (MLA) "Quest Graph™ Four Parameter Logistic (4PL) Curve Calculator" (AAT Bioquest).
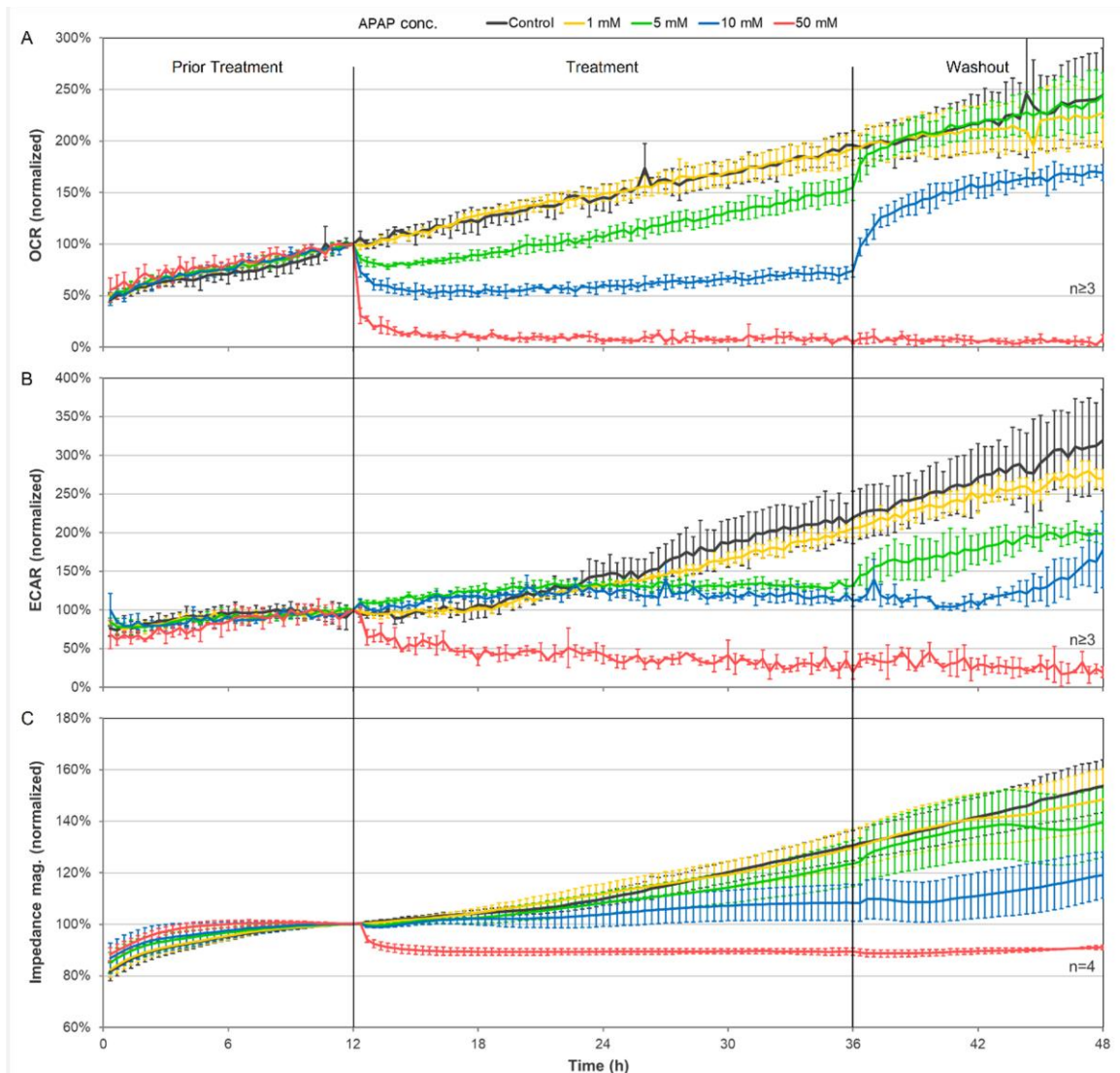
3. Results and Discussion

Figure 2. Normalized metabolic rates and electrical impedance of HepG2 treated with APAP. After prior treatment measurement of HepG2 cells with measurement medium containing 10 % FBS for 12 hours, cells are treated with different concentrations of APAP (0 mM, 1 mM, 5 mM, 10 mM, and 50 mM) for the next 24 hours, followed by a washout of the drug for 12 hours. Shown are the means and standard deviations of metabolic rates for OCR (A) and ECAR (B) and electrical impedance (C) for all treated groups and the untreated control group.

3.1. Oxygen consumption of HepG2 cells under influence of APAP

Measurement of oxygen consumption by HepG2 cells in the presence of APAP showed that the drug decreases the respiration of HepG2 cells in a dose-dependent manner (Figure 2A). The OCR of the control group without treatment steadily increases. The lowest APAP concentration of 1 mM has almost no effect on the cell respiration. The OCR of the groups treated with APAP concentrations above 1 mM decreases significantly during the first hours of treatment. However, as treatment progresses, the OCR of HepG2 cells treated with 5 mM or 10 mM of APAP slowly increases. Thereby, the slope of the increase is the same (5 mM) or lower (10 mM) compared to the control group. The inhibition of respiration of HepG2 cells is most pronounced at the highest APAP concentration of 50 mM. Here, OCR of HepG2 cells reaches its minimum within the first three hours of treatment and remains at this level even after APAP is removed from the medium. HepG2 cells treated with 5 mM or 10 mM APAP regenerate with the washout of APAP, indicated by a marked increase in OCR of these groups. Thereby, the 5 mM group shows full regeneration (OCR equal to control group) whereas the 10 mM group only regenerates to approx. 75 % of the OCR control level. This dose-dependent effect of APAP on the OCR of HepG2 cells is similar to the observations of Thedinga and colleagues in the equivalent APAP concentration range (Thedinga et al 2007). However, our OCR data imply that the treatment of HepG2 cells with low or moderate APAP concentrations (1 mM, 5 mM, or 10 mM) only limits cell growth and does not induce cell death, since the OCR increases steadily, albeit slower, even during treatment. This is in line with our results from impedance measurements and our observations from microscopic images.

It is possible to fit the data from different APAP concentrations at each treatment time point into a four-parameter logistic regression (4PL) to calculate a time-point-specific half maximal effective concentration (EC$_{50}$, Figure 3). Thus, it can be seen that a constant EC50 value of approximately 7.8 mM applies here for OCR almost independent of the exposure time observed.

3.2. Extracellular acidification of HepG2 cells under influence of APAP

The results of acidification measurement also show a time- and dose-dependent change in ECAR by treatment of HepG2 cells with different APAP concentrations (Figure 2B), although it is not as clear as the change in OCR (Figure 2A). Furthermore, the effect of APAP treatment on ECAR is slightly delayed. The treatment group with the lowest concentration (1 mM) again shows only a very small response and the treatment group with the highest concentration (50 mM) a linear decreasing in rate. Both medium concentrations (5 mM and 10 mM) take a similar course during the treatment period. This course is characterized by a brief increase in ECAR above the control group during the first 10 hours of treatment, which then, with no change in activity, falls progressively behind the control. After removal of APAP from the medium the ECAR of HepG2 cells treated with the two medium concentrations (5 mM and 10 mM) rises again, with cells recovering faster after treatment with 5 mM than 10 mM APAP. The effect of the highest APAP concentration was not reversible. Interestingly, our ECAR data show a similar effect of APAP on the acidification behavior of HepG2 cells, as observed by Thedinga and colleagues, when treated with moderate or high APAP concentrations (Thedinga et al 2007). Moreover, our measurement of the acidification implies that APAP treatment decreases the proliferation of HepG2 cells in a dose-dependent manner. After washout of moderate APAP concentrations, both OCR and ECAR of HepG2 cells rises, indicating an

increase in cell proliferation. These observations from metabolic data are supported by impedance measurement and imaging.

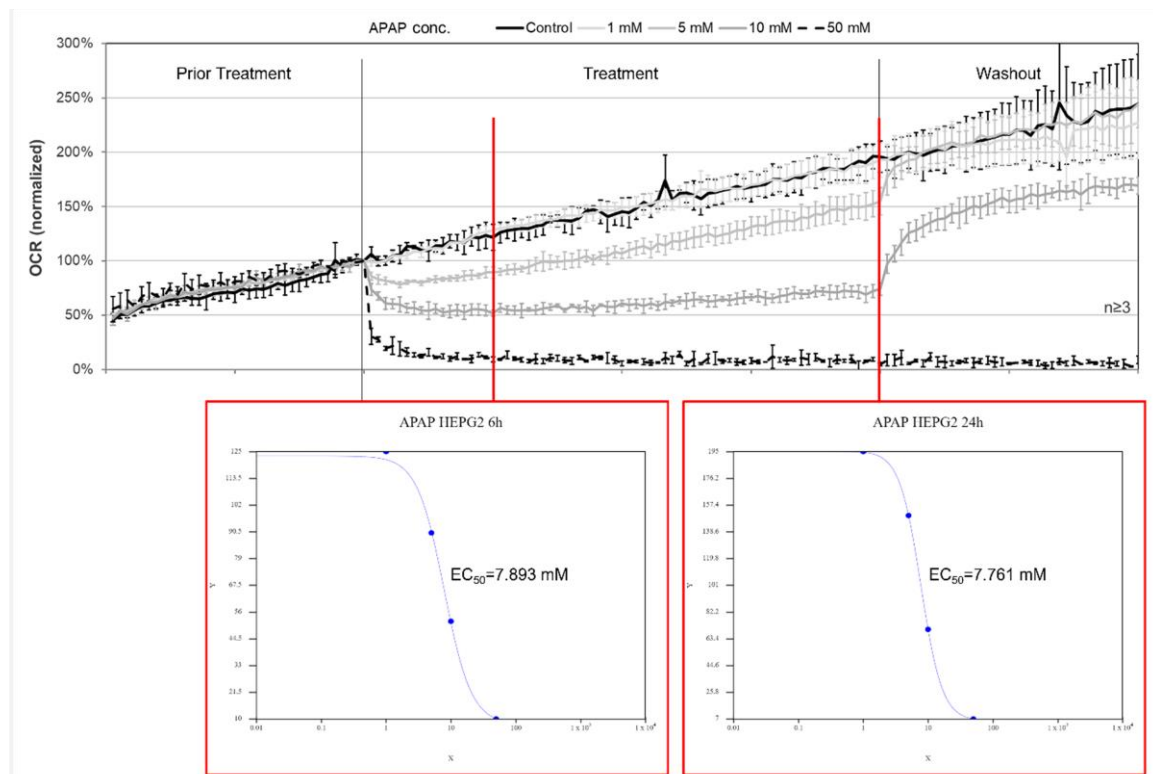### 3.3. Impedance of HepG2 cells under influence of APAP

Figure 3. EC$_{50}$ values of the effect of APAP on HepG2 oxygen consumption. Four-parameter logistic regression (4PL) was used to calculate a time-point-specific half maximal effective concentration (EC$_{50}$) of APAP on HepG2 oxygen consumption. Exemplary EC$_{50}$ values are calculated for two different time points (red boxes), showing the EC$_{50}$ values of the oxygen consumption at 6 hours or 24 hours of APAP treatment. The EC$_{50}$ value for OCR is constant of approx. 7.8 mM and applies almost independently of the exposure time.

Since the increase in cellular impedance after adherence is largely determined by proliferation and the increase in cell density, it can be inferred from the course of impedance that during treatment all groups of HepG2 continue to grow steadily up to a concentration of 10 mM APAP (Figure 2C). However, this is with varying degrees, reflecting a dose-response relationship in which cells proliferate more and more slowly with increasing APAP concentration. In the treatment group with 50 mM APAP, impedance decreases immediately until the end of the treatment period, indicating a loss of cell density and adhesion. After washout of APAP, regeneration of HepG2 cells can be observed again up to a concentration of 10 mM APAP. This differs from the observations of Thedinga and colleagues. Based on impedance data, the authors did not observe regeneration of HepG2 cells during washout of APAP regardless of concentration (Thedinga et al 2007). However, their washout period of 3 hours was much shorter than

our washout period (12 hours). This suggests that a longer washout period should be chosen to observe regeneration processes that require more time. HepG2 cells treated with 50 mM APAP show no signs of recovery. Overall, our results based on the impedance measurement support the metabolic results based on OCR and ECAR measurement. The impedance data demonstrate a dose-dependent effect of APAP on HepG2 cell proliferation, consistent with a slower increase of OCR and ECAR at moderate APAP concentrations compared with the control group.

3.4. Morphology of HepG2 cells under influence of APAP

Automated acquisition of microscopic images of all wells every 20 minutes provides high quality images that allow evaluation of morphological changes throughout the experiment. Repeated micrometer-precise positioning of the microscope makes it possible to track individual cells during the course of the experiment and to view time-lapse videos showing the development of the cultures. Differences in cell migration, which very often occur as a cytotoxic effect, become clearly visible with this tool. At the same time, impedimetric data can be supported and improved by this parallel imaging. Figure 4 shows exemplary images of the same HepG2 cells in a treatment group taken before, during and after treatment with the different APAP concentrations. With increasing APAP concentration, distinct morphological changes of HepG2 cells can be seen. The structural changes are most evident when the cells are treated with 50 mM APAP. Before the addition of APAP, HepG2 cells are adherent, exhibit epithelial morphology and show no obvious signs of stress. After addition of 50 mM APAP HepG2 cells become increasingly inactive and roundish. In addition, the cell-free areas increase. Even during washout of APAP, significant cell degradation can be observed, indicating cell death. These data support the observations from the impedance measurements that 50 mM APAP has toxic effects to HepG2 cells, decreasing cell adhesion and damages the cell layer. Cellular changes such as low proliferation and more cellular inclusions are also observed when 10 mM APAP is applied. However, compared to the 50 mM application, cells recover and return to their original morphological state after washing out APAP. No major morphological changes are seen in HepG2 cells when 1 mM or 5 mM APAP is applied. Overall, the observed morphological changes can be used to support the progression of OCR, ECAR and impedance of HepG2 cells under APAP treatment.
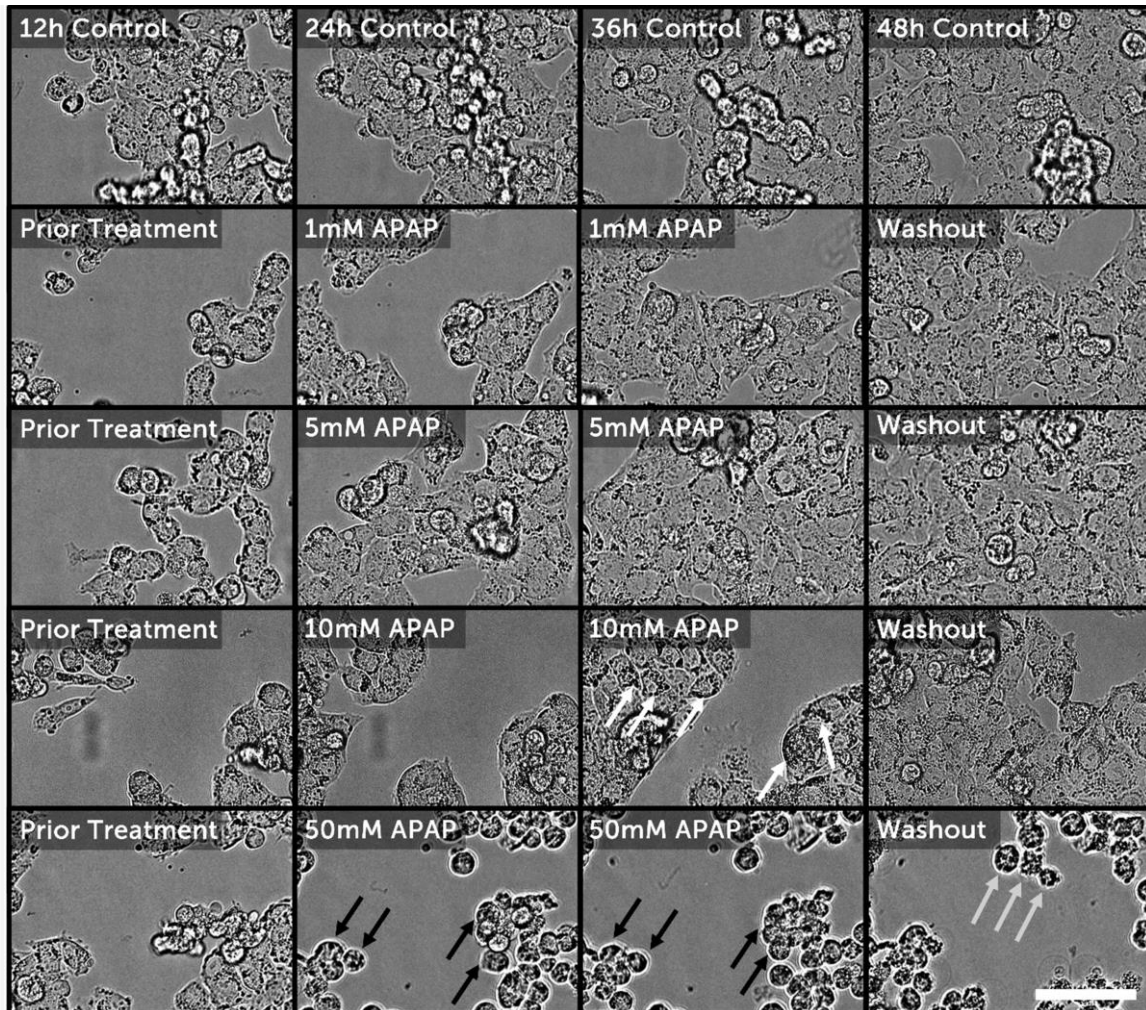
Figure 4. Microscopic images of HepG2 cells treated with APAP. HepG2 cells were preincubated with measurement medium supplemented with 10 % FBS for 12 hours, followed by a treatment with different concentrations of APAP (0 mM, 1 mM, 5 mM, 10 mM, and 50 mM) for 24 hours. APAP was washed out by measurement medium supplemented with 10 % FBS for 12 hours. Microscopic images of all wells were taken every 20 minutes throughout the entire experiment. Based on this overview of microscopic images, morphological differences between the treatment groups can be determined. Up to a concentration of 5 mM APAP, the cells show continuous proliferation over the treatment period. At a concentration of 10 mM APAP, proliferation is very slow and more cellular inclusions are observed (white arrows), but HepG2 cells return to their normal morphology after washout of APAP. When 50 mM APAP is applied, the cells are clearly rounded and detach from the surface (black arrows), and also cell death occurs after APAP washout (gray arrows). The scale bar represents 100 μm.

4. Conclusions

The data of this in-vitro hepatotoxicity assay with HepG2 cells and different APAP concentrations show that the complete dynamics of metabolic and morphologic responses of the cells can be monitored with the CYRIS® FLOX automated cell analysis platform. The metabolic results of the 24-hour treatment showed a strong time- and dose-dependent change of OCR and ECAR, which started at a concentration of 5 mM and became destructive at 50 mM. Interestingly, the metabolic responses of HepG2 cells to treatment with APAP are comparable to those of primary human hepatocytes, as previously demonstrated (Thedinga et al 2007). Morphologic changes monitored by impedance measurement and continuous microscopic imaging underscored these metabolic effects and showed increasing inhibition of cell proliferation. Cell death and detachment were observed only with 50 mM APAP treatment. Post-treatment washout of APAP results in cellular regeneration in all parameters up to a concentration of 10 mM. After treatment with 50 mM APAP no regeneration can be observed in any of the measured parameters. Overall, the results show that the hepatotoxic effect of APAP is particularly pronounced at higher concentrations (50 mM). The continuous measurement of OCR, ECAR, impedance and microscopic images enables real-time multiparametric monitoring of cellular metabolic responses due to APAP treatment in a single assay and is a major advantage of our automated cell analysis platform CYRIS® FLOX. In addition, the temporal density of the data provides an excellent basis for subsequent in-depth analyses, such as the generation of dynamic EC_{50} values and the automatic evaluation of microscopic images. This allows comparison of individual parameters and provides an insightful overall picture of the hepatotoxic effect of APAP on HepG2 cells. A multiparametric approach is crucial to ensure reliable evaluation of the hepatotoxic potential of drugs (Walker et al 2020) because multiple mechanisms are involved in drug-induced hepatotoxicity (Lee 2003). Our automated analysis platform CYRIS® FLOX is a powerful and reliable system to perform multiparametric cell-based assays.

Abbreviations

APAP	Acetaminophen	FBS	fetal bovine serum
OCR	Oxygen consumption rate	DWP	deep well
ECAR	Extracellular acidification rate	w/	with
EC_{50}	Half maximal effective concentration	w/o	without

Acknowledgements

References

Albrecht W, Kappenberg F, Brecklinghaus T et al (2019) Prediction of human drug-induced liver injury (DILI) in relation to oral doses and blood concentrations. Archives of toxicology 93:1609–1637. doi:10.1007/s00204-019-02492-9

AAT Bioquest, Inc, 09 Oct. 2021. https://www.aatbio.com/tools/fourparameter-logistic-4pl-curve-regression-online-calculator

Chen M, Suzuki A, Thakkar, S et al (2016) DILIrank: the largest reference drug list ranked by the risk for developing drug-induced liver injury in humans. Drug discovery today 21:648–653.

doi:10.1016/j.drudis.2016.02.015

Ferrick DA, Neilson A, Beeson C (2008) Advances in measuring cellular bioenergetics using extracellular flux. Drug discovery today 13:268–274. doi:10.1016/j.drudis.2007.12.008

Lee WM, (2013) Drug-induced Acute Liver Failure. Clinics in liver disease 17:575–586. doi:10.1016/j.cld.2013.07.001

Lee WM, (2003) Drug-Induced Hepatotoxicity. The New England journal of medicine, 349:474–485. doi:10.1056/NEJMra021844

Lob V, Geisler T, Brischwein M et al (2007) Automated live cell screening system based on a 24-well-microplate with integrated micro fluidics. Medical and Biological Engineering and Computing 45:1023–1028. doi:10.1007/s11517-007-0260-4

Thedinga E, Ehret R, Schulze M (2007) The Bionas® system bridges the gap between in vivo and in vitro. Nature Methods 4:iii–iv. doi:10.1038/nmeth1071

Thedinga E, Ullrich A, Drechsler S et al (2007) In vitro System for the Prediction of Hepatotoxic Effects in Primary Hepatocytes. ALTEX 24:22-34. doi:10.14573/altex.2007.1.22

Walker PA, Ryder S, Lavado A et al (2020) The evolution of strategies to minimise the risk of human drug-induced liver injury (DILI) in drug discovery and development. Archives of toxicology 94:2559–2585. doi:10.1007/s00204-020-02763-w

Wiest J, Stadthagen T, Schmidhuber M et al (2006) Intelligent Mobile Lab for Metabolics in Environmental Monitoring. Analytical Letters 39:1759-1771. doi:10.1080/00032710600714089

Wolf B, Kraus M, Brischwein M et al (1998) Biofunctional hybrid structures–cell–silicon hybrids for applications in biomedicine and bioinformatics. Bioelectrochemistry and Bioenergetics 46:215–225. doi:10.1016/S0302-4598(98)00169-X

Wolf P, Brischwein M, Kleinhans R et al (2013) Automated platform for sensor-based monitoring and controlled assays of living cells and tissues. Biosensors and Bioelectronics 50:111–117. doi:10.1016/j.bios.2013.06.031